

# Water ice deposition and growth in molecular clouds

Jonathan M. C. Rawlings<sup>★</sup> and D. A. Williams

*Department of Physics and Astronomy, University College London, Gower Street, London WC1E 6BT, UK*

Accepted 2020 November 9. Received 2020 November 9; in original form 2020 August 10

## ABSTRACT

In interstellar clouds, the deposition of water ice on to grains only occurs at visual extinctions above some threshold value ( $A_{\text{th}}$ ). At extinctions greater than  $A_{\text{th}}$ , there is a (near-linear) correlation between the inferred column density of the water ice and  $A_V$ . For individual cloud complexes such as Taurus, Serpens, and  $\rho$ -Ophiuchi,  $A_{\text{th}}$  and the gradients of the correlation are very similar along all lines of sight. We have investigated the origin of this phenomenon, with careful consideration of the various possible mechanisms that may be involved and have applied a full chemical model to analyse the behaviours and sensitivities in quiescent molecular clouds. Our key results are as follows: (i) the ubiquity of the phenomenon points to a common cause, so that the lines-of-sight probe regions with similar, advanced, chemical, and dynamical evolution; (ii) for Taurus and Serpens  $A_{\text{th}}$  and the slope of the correlation can be explained as resulting from the balance of freeze-out of oxygen atoms and photodesorption of  $\text{H}_2\text{O}$  molecules. No other mechanism can satisfactorily explain the phenomenon; (iii)  $A_{\text{th}}$  depends on the local density, suggesting that there is a correlation between local volume density and column density; (iv) the different values of  $A_{\text{th}}$  for Taurus and Serpens are probably due to variations in the local mean radiation field strength; (v) most ice is accreted on to grains that are initially very small ( $<0.01 \mu\text{m}$ ); and (vi) the very high value of  $A_{\text{th}}$  observed in  $\rho$ -Ophiuchi cannot be explained in the same way, unless there is complex microstructure and/or a modification to the extinction characteristics.

**Key words:** astrochemistry – dust, extinction – ISM: molecules.

## 1 INTRODUCTION

Interstellar water ice was first detected in 1973 in the infrared spectra of protostars by absorption in the O–H stretch mode near  $3 \mu\text{m}$  (Gillett & Forrest 1973). Water ice had been sought without success in low-density diffuse regions of interstellar space, but is now well known to be very abundant in dense clouds and star-forming regions where it contains a large fraction of the available oxygen that is not already locked in CO (see the review by van Dishoeck, Herbst & Neufeld 2013, and references therein). Grains of pure ice do not exist; rather, water ice is located as mantles on dust grains of carbon or silicates. It is clear that water ice is formed and retained through reactions on the surfaces of dust grains, rather than the deposition of  $\text{H}_2\text{O}$  molecules from the gas phase (e.g. Jones & Williams 1984; Cuppen et al. 2010; Lamberts et al. 2013). While water is observed to be the dominant component of interstellar ice, other significant component species include CO (deposited directly from the gas phase) and  $\text{CO}_2$  (formed in surface reactions). However, water ice is apparently the first solid material to be deposited on grains.

For any particular interstellar cloud, the observationally determined abundance of the water ice shows two remarkably consistent characteristics as determined from the correlation between the  $3 \mu\text{m}$  optical depth ( $\tau_{3 \mu\text{m}}$ ) and interstellar extinction ( $A_V$ ).

First, it appears that water ice begins to be deposited on dust grains at a critical threshold visual extinction,  $A_V = A_{\text{th}}$  magnitudes, within that cloud (Whittet et al. 2013). Although there is some scatter in

the vicinity of  $A_{\text{th}}$ , this value is well defined, so that, although  $A_{\text{th}}$  varies from cloud to cloud, cores within each cloud complex have the same value of  $A_{\text{th}}$  with very few outliers. Below this cut-off value,  $\tau_{3 \mu\text{m}} = 0$ , i.e.  $\text{H}_2\text{O}$  ice is not present. Ice deposition in the quiescent dark cloud in Taurus has been extensively studied (Whittet et al. 1989, 2001, 2007; Chiar et al. 1994; Bergin et al. 2005) and the critical value of visual extinction for ice deposition in that cloud is  $3.2 \pm 0.1 \text{ mag}$ . A study of the quiescent dark cloud complex IC 5146 finds the same critical value (Chiar et al. 2011), implying a common mechanism in regions that do not possess internal heating/radiation sources. However, on other lines of sight, particularly those in star-forming regions, the critical value may be significantly larger, for example, in the active star-forming Serpens cloud the critical value of visual extinction is  $\sim 6 \text{ mag}$ , while in the intermediate-/high-mass star-forming region of  $\rho$ -Ophiuchus it is  $\sim 13 \text{ mag}$  (Whittet & Blades 1980; Eiroa & Hodapp 1989; Tanaka et al. 1990).

Threshold extinctions have also been determined for other ice components, such as CO and  $\text{CO}_2$ , as well as for complex organic molecules (COMs), although these are typically more variable and larger (especially for the COMs) as compared to that for water ices.

Secondly, on paths with visual extinctions greater than the critical value, the quantity of ice as measured by the optical depth at  $3 \mu\text{m}$  rises almost linearly with  $A_V$  (Whittet et al. 1989; see also Whittet 2003, for a summary), and the value of the slope of the plot of  $\tau(3 \mu\text{m})$  versus  $A_V$ , which we denote by  $\alpha_{\text{H}_2\text{O}}$ , appears to be very similar in each case. Thus,  $\alpha_{\text{H}_2\text{O}} = 0.072 \pm 0.002$  and  $0.068 \pm 0.003$  for IC 5146 and Taurus, respectively (Whittet et al. 2001; Chiar et al. 2011), although Chiar et al. (2007, 2011) also note that the slope is generally shallower in dense clouds than it is in more diffuse

<sup>★</sup> E-mail: jcr@star.ucl.ac.uk

clouds. The similarity of the slopes might imply that all available oxygen has been converted to water ice. However, as we discuss below, differences in astrophysical parameters such as local density and local metallicity would be expected to have significant effects.

While ice deposition has received much theoretical attention (e.g. Cuppen & Herbst 2007; Andersson & van Dishoeck 2008; Ioppolo, Cuppen & Romanzin 2008; Du, Parise & Bergman 2012; Kalvāns 2015), the actual processes controlling the onset of ice deposition and the removal of H<sub>2</sub>O molecules from ice remain a matter for discussion.

A number of studies have addressed the issue of the  $A_{\text{th}}$  phenomenon and have usually invoked the obvious  $A_V$ -dependence of photodesorption of ices as the most likely cause, although there has been little attempt to explain (a) its value and universality within molecular clouds, and (b) why it varies between clouds. In addition, there are other possible causes for the phenomenon that are not directly related to the photodesorption effect that should also be considered.

In a study of the effects of selective desorption mechanisms on the growth and composition of interstellar ices, Kalvāns (2015) developed a comprehensive model of the processes on and in (the top four layers) of ices including the full range of desorption processes that we describe in this paper, surface chemistry, diffusion, and the chemistry in sublayers together with considerations of the mobility of species on the surface and within the ices. The model examined the time-dependencies of the ice abundances (the main components, and also the complex organics), in the context of a simple isothermal free-fall collapse model, so that – in this model – the extinction is directly related to the dynamical age, although a complicating factor is introduced here in that, as the collapse proceeds, the dynamical time-scale becomes significantly shorter than the chemical time-scale. The paper showed the relative importances of photodesorption and reactive desorption processes in determining the efficiency of freeze-out and the composition of the ices. A value of  $A_{\text{th}} \sim 8 - 10.5$  is determined for CO ices, although the work does not specifically address the issue of the determination and variation of the critical extinction for H<sub>2</sub>O ices.

A number of other mechanisms have recently been proposed concerning the deposition of interstellar ice, in addition to studies of the type discussed in the papers listed above. In this paper, we wish to examine the various proposals, with a view to addressing the following questions:

- (i) What are the physical conditions that determine the critical extinction for ice deposition, and why is  $A_{\text{th}}$  the same along different sightlines in the same cloud complex?
- (ii) Why is there a wide range of  $A_{\text{th}}$  in different clouds?
- (iii) Can a single mechanism account for the observed wide range of  $A_{\text{th}}$  in different clouds?
- (iv) Can any of the suggested mechanisms limiting ice deposition be discounted?
- (v) What determines the slope of the  $\tau(3\ \mu\text{m})$  v.  $A_V$  plot ( $\alpha_{\text{H}_2\text{O}}$ ), and why is a single correlation apparently applicable to many sources, with little scatter?
- (vi) Can we use information contained in the value of  $A_{\text{th}}$  and  $\alpha_{\text{H}_2\text{O}}$  to determine the physical conditions where ice deposition is occurring?

As the empirical basis for testing our hypotheses and models, we use the data summarized in Whittet et al. (2013). They argue that the optical depth in the 9.7  $\mu\text{m}$  silicate absorption feature is the best proxy for the dust column density and deduce a value of  $A_{\text{th}} = 2.7 \pm 0.5$  for H<sub>2</sub>O for the combined data sets for L183, Taurus, and

IC5146. In addition, the correlation between  $N(\text{H}_2\text{O})$  and  $\tau_{9.7\ \mu\text{m}}$  is linear and remarkably similar for the three sources, and from fig. 14 of that paper we can therefore also deduce that

$$N(\text{H}_2\text{O}) \sim 2.05 \times 10^{17} (A_V - 2.7) \text{ cm}^{-2}. \quad (1)$$

This correlation has remarkably little scatter, and there is little variation of either  $A_{\text{th}}$  or  $\alpha_{\text{H}_2\text{O}}$  between the three sources that are compared in that paper (the quiescent, chemically evolved pre-stellar core L183 (L134N), Taurus, and IC 5146).

In the discussion that follows, we must recognize that the observed (i.e. line of sight) extinction to a source is not necessarily the same as the ‘local’ extinction, that is, to say the extinction of the source relative to the interstellar radiation field, so there will always be some uncertainty/natural scatter in the values of  $A_{\text{th}}$ . However, the near-universality of these dependencies implies that the relevant processes must be largely independent of the dust properties; such as the size distribution and the dust grain morphology and porosity, etc.

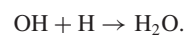
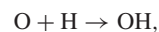
In the following section, we describe the nature of interstellar ices and the criterion for ice mantle growth. In Section 3, we describe the various microscopic mechanisms that determine  $A_{\text{th}}$ , and in Section 4 we compare the relative importances of these processes. Section 5 describes our chemical model, and the results are presented in Section 6. Possible alternative causes of the  $A_{\text{th}}$  phenomenon are discussed in Section 7. Our conclusions and discussion are presented in Section 8.

## 2 THE REQUIREMENT FOR ICE MANTLE GROWTH

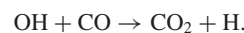
Interstellar ices are predominantly composed of H<sub>2</sub>O, CO, and CO<sub>2</sub>, with CO and CO<sub>2</sub> having abundances of  $\sim 27-32$  per cent and  $\sim 19$  per cent, respectively, relative to H<sub>2</sub>O in Taurus and low-mass young stellar objects (YSOs) (Chiar et al. 2011, table 4). CO, being more volatile, is typically less abundant in high mass YSOs. Other species (such as CH<sub>3</sub>OH, NH<sub>3</sub>, OCN<sup>-</sup>, and other organics/COMs) typically account for  $\lesssim 10$  per cent of the ice.

The relative abundances of the major ice components are fairly similar in different environments, although real differences exist and there are often significant variations in the abundances of the complex organics. Whilst there is evidence for significant source to source variations in the relative abundances of H<sub>2</sub>O, CO, and CO<sub>2</sub>, the total contribution of O-bearing ice molecules to the oxygen budget follows similar trends in different sources (e.g. Whittet et al. 2009).

The chemistry of the main components is straightforward; CO ice is believed to be formed (primarily) due to the freeze-out of CO from the gas phase. By contrast, H<sub>2</sub>O and CO<sub>2</sub> are probably formed by surface reactions. At least four distinct H<sub>2</sub>O formation mechanisms are possible (van Dishoeck et al. 2013), but in the relatively low density/high hydrogen atom abundance environments that we are considering in this study, the main channel is simple hydrogenation:



The latter reaction being in competition with



As gas-phase chemistry is not believed to be important, this means that the formation rate of H<sub>2</sub>O ice is mainly determined by the rate at which oxygen atoms stick to grains and are subsequently hydrogenated to H<sub>2</sub>O molecules. If these are the only relevant

reactions, then it also follows that the abundances of H<sub>2</sub>O and CO<sub>2</sub> ice should be approximately correlated, which is indeed seen to be the case (e.g. Noble et al. 2013).

Ultimately, whatever mechanism(s) is/are at play, the abundances of ices on grains and the explanation for the  $A_{\text{th}}$  phenomenon must be determined by the balance between the freeze-out/formation of H<sub>2</sub>O and its desorption, perhaps coupled with observational biasing and line-of-sight effects.

We can therefore deduce the criterion for efficient ice formation as follows: the rate at which a species freezes-out on to dust grain surfaces obviously depends on the available surface area. We make the assumptions that (i) the ice composition is dominated by H<sub>2</sub>O, and (ii) desorption from the ice mantle is dominated by processes that occur at the surface (as would be the case for photodesorption or desorption following H<sub>2</sub> formation). The desorption rate then depends on the fractional composition of the top monolayer(s) of the ice and scales linearly with the fractional coverage of the surface of the grains by H<sub>2</sub>O ( $f_{\text{H}_2\text{O}}$ ).

If  $f_{\text{H}_2\text{O}}$  reaches unity (i.e. total surface coverage in a monolayer of a pure ice composition), then the desorption rate will saturate. If the freeze-out and desorption rates are balanced at a level corresponding to  $f_{\text{H}_2\text{O}} < 1$ , then clearly, an ice mantle will not grow; the net freeze-out is quenched before a monolayer of ice can be formed.

If on the other hand, when  $f_{\text{H}_2\text{O}}$  reaches 1 and the desorption rate is less than the freeze-out rate, then continual mantle growth will occur. Indeed, as the mantle grows the effective surface area grows and the rate of growth will accelerate (the ‘snowball’ effect). The imbalance between desorption and freeze-out will be further enhanced by the fact that the binding energy of water molecules to ice is larger, due to strong hydrogen bonding, than it is for bare carbon or silicate grains (Williams, Hartquist & Whittet 1992).

Thus, the criterion for ice mantle growth is that the desorption rate at  $f_{\text{H}_2\text{O}} = 1$  must be less than the freeze-out rate. If  $f_{\text{H}_2\text{O}} = 1$  can be reached, then rapid ice mantle growth will ensure. This condition can be used to define  $A_{\text{th}}$ .

### 3 MECHANISMS AND PROCESSES THAT MAY DETERMINE THE CRITICAL EXTINCTION

Various non-thermal mechanisms have been suggested as having a defining role in determining the critical visual extinction for the deposition of ice on dust grains. These include

- (i) Non-thermal, continuous desorption,
- (ii) The dependence of the H<sub>2</sub>O-grain surface binding energy on  $A_V$ ,
- (iii) The requirement for a critical O-atom flux at grain surfaces, and
- (iv) Variations in the efficiencies of surface chemistry.

In this study, we describe these mechanisms and assess their viability as a cause of the  $A_{\text{th}}$  phenomenon. First, we need to identify and quantify the various microscopic processes that may determine the abundance of H<sub>2</sub>O ices. These include (a) gas-phase formation (and destruction), (b) photodissociation, (c) freeze-out, (d) surface chemistry (forming H<sub>2</sub>O, as described above, and also including photodissociation of the ices), and (e) desorption. Of these, (a) and (b) are probably relatively unimportant as explained above, whilst (c)–(e) depend on a number of parameters, including the local temperature, density, radiation field strength, available dust grain surface area, desorption yields, surface coverage of dust grains by the various ice components etc. It is therefore quite remarkable that a single

ice band-extinction correlation exists. This tells us that whatever the physical origin of  $A_{\text{th}}$  is, it must be very robust to any assumptions that we make, or variabilities that exist, in the grain physics and the chemical processes involved.

We now discuss the specific processes and assess their range of relevance/applicability, before identifying the possible dependencies on  $A_V$ .

#### 3.1 Freeze-out

Following Rawlings et al. (1992), the rate of decline ( $\text{cm}^{-3}\text{s}^{-1}$ ) of the abundance of a gas-phase species,  $i$ , due to freeze-out can be written as

$$\dot{n}_i = - \left( \frac{k}{2\pi m_H} \right)^{\frac{1}{2}} \sigma_H S_i C \left( \frac{T_{\text{gas}}}{m_i} \right)^{1/2} n_H n_i, \quad (2)$$

where  $n_H$  is the hydrogen nucleon density ( $\text{cm}^{-3}$ ),  $S_i$  is the sticking coefficient (in the range 0–1),  $T_{\text{gas}}$  is the gas kinetic temperature,  $m_i$  is the molecular mass of species  $i$  in  $amu$ , and  $C$  is a factor that takes into account electrostatic effects (and is a function of the grain size, as defined in Rawlings et al. 1992). For neutral species, such as H<sub>2</sub>O and CO,  $C = 1$ .  $\sigma_H$  is the grain population-averaged value of

$$4\pi \bar{a}^2 d_g,$$

where  $\bar{a}$  is the mean grain radius and  $d_g$  is the dust-to-gas ratio (by number, relative to  $n_H$ ) and is effectively the mean ‘surface area of dust grains per hydrogen nucleon’. The factor of 4 in this expression implicitly assumes that the grains are spherical.

$\bar{a}$ , and  $\sigma_H$  are important independent parameters in this study and in the models described below. The significance of  $\bar{a}$ , particularly in the determination of  $\sigma_H$ , becomes particularly apparent when the effects of ice mantle growth are taken into effect; thus, although the values of  $A_{\text{th}}$  and the number of accreted ice monolayers are not expected to be sensitive to  $\bar{a}$ , smaller values of  $\bar{a}$  will result in a more rapid increase in  $\bar{a}$  and  $\sigma_H$  as ice mantles grow; which can be termed the ‘snowball effect’. So, for example, the growth of 50 monolayers of ice each of the same thickness) would typically result in an increase of the surface area by factors of  $\sim 22$  and  $\sim 1.4$  for grains whose bare radius is 0.01 and 0.1  $\mu\text{m}$ , respectively.

If we adopt the standard power-law grain size distribution for interstellar dust (Mathis, Rumpl & Nordsieck 1977), then  $\bar{a} \sim 0.008 \mu\text{m}$ , the RMS value is  $\bar{a}^{1/2} \sim 0.01 \mu\text{m}$  (appropriate for determining  $\sigma_H$ ), the median value of the grain surface area distribution is  $\sim 0.018 \mu\text{m}$  and  $\sigma_H \approx 3.3 \times 10^{-21} \text{cm}^2$ . These values are highly uncertain, due to the assumptions about grain composition, morphology, and the effects of grain aggregation and/or thick ice mantle accretion, but in any case it is clear that most of the surface area of the population resides in the smallest grains.

This value of  $\bar{a}$  is significantly smaller than the value of  $\sim 0.1 \mu\text{m}$  that is adopted in many studies (e.g. Taquet, Ceccarelli & Kahane 2012; Kalvāns 2015). Those studies often cite the likelihood of dust grain agglomeration in dense environments but, if such processes are relevant, they will also have very strong – and usually neglected – effects on both  $\sigma_H$  and the UV opacity and hence the  $A_V$ -dependence of the photoreaction rates.

In the context of our discussion, it is also useful to define  $f_{\text{sites}}$ , the effective fractional abundance (relative to hydrogen nucleons) of binding sites:

$$f_{\text{sites}} = \sigma_H \cdot N_s,$$

**Table 1.** Standard parameters in the model.

Parameter	Description	Value
$C/H$	Total carbon abundance	$3.0 \times 10^{-4}$
$O/H$	Total oxygen abundance	$5.0 \times 10^{-4}$
$X(CO)_0$	Initial fractional abundance of CO	$2.7 \times 10^{-4}$
$T_{\text{gas}}$	Gas temperature	10 K
$T_{\text{dust}}$	Dust temperature	10 K
$\omega$	Grain albedo	0.5
$\bar{a}$	Average grain radius	$8.3 \times 10^{-3} \mu\text{m}$
$\sigma_{\text{H}}$	Dust surface area per H nucleon	$3.3 \times 10^{-21} \text{cm}^2$
$\Delta a$	Ice monolayer thickness	3.7 Å
$S_{\text{eff, O}}$	Effective sticking and conversion coefficient (O $\rightarrow$ H <sub>2</sub> O)	1.0
$F_0$	Unshielded IS photon flux	$1.0 \times 10^8 \text{photons cm}^{-2} \text{s}^{-1}$
$F_{\text{CR}}$	Cosmic-ray-induced photon flux	$4875.0 \text{photons cm}^{-2} \text{s}^{-1}$
$\zeta$	Cosmic ray ionization rate/ $1.3 \times 10^{-17} \text{s}^{-1}$	1.0
$R_{\text{CR}}$	Cosmic ray desorption rate for H <sub>2</sub> O	$4.40 \times 10^{-17} \text{s}^{-1}$
$Y_{\text{pd, i}}$	Photodesorption yield	$1.0 \times 10^{-3}$
$Y_{\text{pd-cr, i}}$	Cosmic ray induced photodesorption yield	$1.0 \times 10^{-3}$
$Y_{\text{H}_2, \text{i}}$	Yield for desorption by H <sub>2</sub> formation	0.0
$G$	ISRF/Draine	1.0
$N_{\text{s}}$	Grain binding site surface density	$1.0 \times 10^{15} \text{cm}^{-2}$
$E_{\text{bind}}/k$	H <sub>2</sub> O binding energy/k	4,800 K

where  $N_{\text{s}}$  is the mean surface density of binding sites on grains. Thus, the surface coverage of a monolayer is given by the sum of the fractional abundances of solid-state species divided by  $f_{\text{sites}}$ .

In the absence of any desorption processes, we can calculate (from equation 2, above) a characteristic freeze-out time-scale for oxygen atoms (for which  $\mu = 18$ );  $\tau_{\text{fo}}$ .  $\tau_{\text{fo}}$  is defined as the time required for the change in the abundance of gas-phase oxygen atoms to be comparable to the initial abundance. Thus,

$$\tau_{\text{fo}} = 1.1 \text{Myr} \left( \frac{10^{-20} \text{cm}^{-2}}{\sigma_{\text{H}}} \right) \left( \frac{10}{T_{\text{gas}}} \right)^{1/2} \left( \frac{10^3 \text{cm}^{-3}}{n_{\text{H}}} \right) \text{yr}. \quad (3)$$

Note the somewhat counterintuitive result that (assuming the dust grains are sufficiently cold for thermal desorption not to occur), higher gas temperatures result in faster freeze-out.

In reality, the ‘effective’ sticking coefficient must take account of the following:

- The sticking efficiency of O atoms, OH radicals, and H<sub>2</sub>O (and O<sub>2</sub>) molecules,
- Surface reaction efficiencies for the conversion of O and OH to H<sub>2</sub>O, and
- Desorption driven by the enthalpy of surface reactions.

For (a) it is probably fair to assume that the sticking probabilities are of order unity. For (b), reactions involving the hydrogenation of O, OH (and O<sub>2</sub>) usually lead to H<sub>2</sub>O formation. We recognize that the efficiencies are poorly constrained, and so we investigate a range formation efficiencies of 0–100 per cent, whilst for (c) we are guided by the empirical and theoretical studies of Minissale et al. (2016). The enthalpy of formation may result in the desorption of the product species and the chemical desorption efficiencies for the O+H $\rightarrow$ OH reaction were determined to be  $\sim$ 50 per cent on oxidised graphite, and  $\sim$ 25 per cent on amorphous water ice. For the OH+H $\rightarrow$ H<sub>2</sub>O reaction, the desorption efficiencies are  $\sim$ 50 per cent,  $\sim$ 80 per cent, and  $\sim$ 30 per cent for oxidized graphite, amorphous silicates, and amorphous water ice, respectively. These imply a reduced net sticking/reaction efficiency for oxygen atoms and OH radicals.

### 3.2 Thermal desorption

The rate of thermal sublimation (per molecule) for a zeroth order process is given by

$$k = \nu_0 e^{-E_{\text{bind}}/k_{\text{B}} T_{\text{dust}}} \text{s}^{-1},$$

where  $E_{\text{bind}}$  is the binding energy of the adsorbate,  $T_{\text{dust}}$  is the dust temperature, and  $\nu_0$  is the vibration frequency of the adsorbed molecule. Due to the exponential dependence on the dust temperature, thermal desorption effectively operates as an on/off switch at a characteristic temperature defined by the balance between freeze out and thermal desorption. For H<sub>2</sub>O, if we balance the desorption rate with the freeze-out rate for oxygen atoms (assuming an effective sticking/hydrogenation coefficient of 1, a gas temperature of  $\sim$ 10 K and values for  $N_{\text{s}}$  and  $E_{\text{bind}}$  as given in Table 1), then the critical balance ( $f_{\text{i}} = 1$ ) is obtained for

$$T_{\text{dust}} \sim \frac{4800}{55 - \ln n(\text{O})}, \quad (4)$$

where  $n(\text{O})$  is the gas-phase density of oxygen atoms, implying that thermal desorption is only efficient for  $T_{\text{dust}} > > 10$  K. It is therefore entirely suppressed for the conditions that exist within molecular clouds, and is only a significant mechanism in the close vicinity of protostars, when the requisite temperatures of  $T_{\text{dust}} \sim 100$  K can be obtained. By contrast, thermal desorption is much more important in molecular clouds for species such as CO, which are more volatile and have much lower surface binding energies.

### 3.3 Cosmic-ray-induced desorption

The rate of desorption of a species as a result of cosmic ray heating of grains and ice mantles (whether in localized hotspots or whole grain heating) can be expressed as

$$\dot{n}_{\text{i}} = R_{\text{cr}} n_{\text{i}},$$

where  $R_{\text{cr}}$  is the cosmic ray desorption rate per molecule and  $n_{\text{i}}$  is the volume abundance of the solid-state species (e.g. Hasegawa & Herbst 1993). Importantly, the action of cosmic rays is not necessarily

limited to the surface layers of the ices, so – unlike photodesorption – this rate depends on the total abundance of species in the ice and not just the surface coverage. For the purpose of our numerical calculations, note that in the critical case of  $f_{\text{H}_2\text{O}} = 1$  (and, again, assuming a pure water ice),  $n_{\text{H}_2\text{O}}$  is given by  $\sigma_{\text{H}}N_{\text{s}}n_{\text{H}}$ .

Until recently, calculations of the cosmic ray desorption rates have included a number of simplifications including the assumptions that (a) dust grains are spherical with high thermally conductivity, (b) the process is limited to larger (0.1  $\mu\text{m}$ ), classical grains, (c) the various ice components co-desorb with characteristics defined for binding energies for simple, pure compositions, and (d) the cosmic ray energy spectra are idealized and invariant. However, as is shown below, cosmic ray desorption is not likely to be a major contributor to the total  $\text{H}_2\text{O}$  desorption rate, so these issues are not relevant in this study.

The negligible importance of cosmic ray heating also seems to be supported by the findings of Whittet et al. (2013) who, in their study of L183, found that the ices are amorphous in structure, indicating that they have not been heated to  $\gtrsim 15$  K since their formation. This would seem to be consistent with the fact that – for this source at least – whole grain heating by cosmic rays is not an effective desorption mechanism, unless the annealing effects of cosmic ray heating can be mitigated by exposure to amorphizing UV radiation (e.g. Leto & Baratta 2003).

### 3.4 Photodesorption

Photodesorption from water ice initiated by the interstellar UV radiation field provides an obvious explanation for the  $A_{\text{th}}$  phenomenon; the photodesorption rate declines with depth into the cloud, so that at the cloud edge, photodesorption dominates over freeze-out and inhibits ice deposition, but at a sufficient depth, corresponding to  $A_{\text{V}} = A_{\text{th}}$ , freeze-out dominates over photodesorption and ice mantles begin to form.

The photodesorption rate has been measured in the laboratory (e.g. Westley et al. 1995; Yabushita et al. 2006; Öberg et al. 2009) and has been the subject of many classical molecular dynamics simulations. The process involves the photodissociation of an  $\text{H}_2\text{O}$  molecule in the ice into energetic H and OH radicals that may recombine, escape, or be trapped in the ice lattice; the process depends on the depth within the ice of the dissociated molecule (Andersson & van Dishoeck 2008).

The photodesorption flux ( $\text{cm}^{-2}$ ) of a species  $i$  is given by (e.g. Hollenbach et al. 2009)

$$F_{\text{pd},i} = Y_{\text{pd},i} F_{\text{UV}} f_i, \quad (5)$$

where  $Y_{\text{pd},i}$  is the photodesorption yield for species  $i$  and  $F_{\text{UV}}$  is the photon flux. The rate of desorption of species  $i$  is then given by

$$\dot{n}_i = \sigma_{\text{H}} n_{\text{H}} F_{\text{pd},i}, \quad (6)$$

where  $\sigma_{\text{H}} n_{\text{H}}$  is effectively the grain surface area per unit volume of the gas. The photon flux is given by

$$F_{\text{UV}} = G F_0 e^{-1.8A_{\text{V}}} + 4875.0\zeta. \quad (7)$$

In this expression, the first term accounts for direct photodesorption;  $F_0$  is the unshielded interstellar UV flux, with a scaling factor  $G$  and the exponential accounts for shielding by dust. The second term accounts for cosmic-ray-induced photodesorption;  $\zeta$  is a scaling factor for the cosmic ray ionization rate and is normalized to the ‘standard’ value of  $\zeta_0 = 1.3 \times 10^{-17} \text{s}^{-1}$ .

$Y_{\text{pd},i}$  and  $f_i$  are both uncertain.  $Y_{\text{pd},i}$  has been measured in the laboratory to be  $\sim 10^{-4} - 10^{-3}$  but this is for pure water ices on a flat

gold substrate. It would seem unlikely that the same values would apply to impure/mixed ices on amorphous and morphologically complex grain surfaces. It is also apparent that photodesorption is intrinsically a surface process which affects only the top few (maybe 3 or 4) monolayers of an ice mantle. To calculate the photodesorption rate therefore requires a knowledge of the composition of the ices on a layer-by-layer basis. The calculation of the fraction of surface binding sites that are occupied by a species ( $f_i$ ) is non-trivial and requires a knowledge of the morphology and accretion history of individual ice mantles, as well as taking account of the adsorption and desorption rates of all of the dominant ice constituents. Unless there is complete fluid mixing within the ice  $f_i$  is *not* the same as the bulk mantle fractional composition of species  $i$ .

### 3.5 Surface chemistry – chemically driven desorption

We have considered two mechanisms for desorption driven by the enthalpy of formation of molecules in surface reactions:

(a) selective desorption of the product molecules (OH and  $\text{H}_2\text{O}$ ) in surface hydrogenation reactions, and

(b) non-selective desorption of molecules driven by the formation of  $\text{H}_2$  on surfaces.

We have discussed the first of these in subsection 3.1 above, where we treat the process as effectively modifying the freezeout/reaction rate of O and OH. For the second, we know that the formation of  $\text{H}_2$  molecules on the surface of dust grains results in an energy deposit into the grain that is a significant fraction of the  $\text{H}_2$  bond energy (4.5 eV). Such a large energy input will be capable of desorbing molecules, possibly non-selectively, in the vicinity of an  $\text{H}_2$  formation site, although the efficiency of that desorption is highly uncertain.

If we make the reasonable assumption that the desorption is a surface process (i.e. effecting desorption from the surface layer(s) of the ice mantle), then we can write the rate of desorption ( $\text{cm}^{-3} \text{s}^{-1}$ ) of a species  $i$  as

$$\dot{n}_i = Y_{\text{H}_2,i} \dot{n}_{\text{H}_2} f_i, \quad (8)$$

where  $Y_{\text{H}_2,i}$  is the desorption yield for species  $i$ ,  $f_i$  is the surface coverage of species  $i$ , as above, and  $\dot{n}_{\text{H}_2}$  is the rate of (surface)  $\text{H}_2$  formation. Of course,  $\dot{n}_{\text{H}_2}$  is determined by the H-atom abundance that will itself be a function of  $A_{\text{V}}$ .

For the purpose of this study, we can then speculate that the  $A_{\text{V}}$ -dependence of ice formation may result from the variation in the abundances of O and H atoms with density and depth into a cloud. As the H to  $\text{H}_2$  abundance ratio declines with depth so too will the  $\text{H}_2$ -formation driven  $\text{H}_2\text{O}$  desorption rate until a point is reached (at  $A_{\text{V}} = A_{\text{th}}$ ) at which it is less than the net accretion rate. If this were to prove a viable mechanism then, as the desorption yield is unknown, the observed value(s) of  $A_{\text{th}}$  could be used to predict the value(s) of  $Y_{\text{H}_2,i}$ .

Thus, balancing the expressions for freeze-out and chemical desorption rates given above, we see that (if chemical desorption is the main process that determines whether or not ices form) then the critical condition corresponding to  $A_{\text{V}} = A_{\text{th}}$  is given by

$$\frac{n_{\text{O}}}{n_{\text{H-atoms}}} = 2Y_{\text{H}_2,\text{H}_2\text{O}} \left( \frac{S_{\text{eff,H}}}{S_{\text{eff,O}}} \right), \quad (9)$$

where  $S_{\text{eff,O}}$  and  $S_{\text{eff,H}}$  are the effective sticking and the hydrogenation efficiencies for oxygen and hydrogen atoms, respectively. We assume these are of order unity and that the process is non-selective, to the extent that it results in the desorption of strongly bound species, like  $\text{H}_2\text{O}$  (an assumption that may not be valid e.g. Roberts et al. 2007) and that the abundance of hydrogen atoms is  $\sim 1 \text{ cm}^{-3}$  in

molecular clouds. With these assumptions, this implies that whilst H<sub>2</sub>-formation-driven desorption may be important in maintaining a significant gas-phase abundance of H<sub>2</sub>O at high extinctions, it is only important in the determination of the abundance of solid-state H<sub>2</sub>O when the density of oxygen atoms is  $\lesssim 0.5Y_{\text{H}_2, \text{H}_2\text{O}}$ . With  $Y_{\text{H}_2, \text{H}_2\text{O}} \sim 10^{-4} - 10^{-3}$ , this condition is unlikely to be satisfied in normal circumstances.

#### 4 ANALYTICAL CONSIDERATIONS

Adopting the standard values for the parameters as specified in Table 1, we find that the rates per hydrogen nucleon for the various desorption processes for H<sub>2</sub>O; thermal, cosmic ray heating, direct photodesorption, cosmic-ray-induced desorption and desorption driven by the enthalpy of H<sub>2</sub> formation are  $\sim 0$ ,  $1.45 \times 10^{-22}$ ,  $3.3 \times 10^{-16} e^{-1.8A_V}$ ,  $1.6 \times 10^{-20}$ , and  $1.9 \times 10^{-17} Y_{\text{H}_2}$ , respectively. For comparison, the representative freeze-out rate is  $9.5 \times 10^{-18} n_{\text{O}}$ . From these values, we can see that, at low extinctions, direct photodesorption is by far the dominant desorption mechanism.

However, as previously noted by Williams et al. (1992) this result does not hold at higher extinctions. For example, with  $A_V = 10$ , the extinction in the UV absorption band for H<sub>2</sub>O dissociation ( $h\nu \sim 7 - 10$  eV) is  $\sim 30$  magnitudes for a conventional interstellar extinction curve, so that external radiation fields are effectively excluded. In that case, photodesorption driven by the ( $A_V$ -independent) cosmic-ray-induced UV radiation field (Prasad & Tarafdar 1983) becomes the dominant photodesorption mechanism, at almost unlimited depths in clouds or star-forming regions.

From equation 7 in subsection 3.4, above we can quantify this; cosmic-ray-induced photodesorption dominates (and the desorption rate effectively ceases to have an explicit dependence on  $A_V$ ) once

$$A_V > 5.51 + 0.56 \ln \left( \frac{G}{\zeta} \right). \quad (10)$$

Thus, whilst the  $A_V$ -dependence can be invoked to explain  $A_{\text{th}}$  in Taurus and Serpens, it cannot for  $\rho$ -Oph (where it would imply a value of  $G/\zeta > 10^5$ ).

Balancing the rate of freeze-out of oxygen atoms with the rate of photodesorption of H<sub>2</sub>O molecules (and neglecting the term due to cosmic ray induced photodesorption) we obtain, with the value of  $F_0$  given in Table 1 and for  $f_i = 1$ :

$$A_V = 1.97 + 0.56 \ln \left( G \frac{Y_{\text{pd}}}{10^{-3}} \right) - 0.56 \ln (S_{\text{eff}, \text{O}} n_{\text{O}}) - 0.28 \ln \left( \frac{T_{\text{gas}}}{10} \right), \quad (11)$$

From this expression, we can see that, in regions where photodesorption is the dominant desorption process,  $A_{\text{th}}$  is primarily dependent on the values of  $G$ ,  $Y_{\text{pd}}$ ,  $S_{\text{eff}, \text{O}}$ , and  $n_{\text{O}}$  (and hence the C:O ratio and the C-to-CO conversion efficiency – see below). The dependence on  $T_{\text{gas}}$  is less significant as the range of uncertainty in the parameter is smaller than for those listed above.

If we adopt  $G = 1$ ,  $Y_{\text{pd}} = 10^{-3}$  (as in Table 1),  $S_{\text{eff}, \text{O}} = 1$  and  $T_{\text{gas}} = 10$  then this formula implies that, to obtain  $A_{\text{th}} > 0$ , the oxygen atom abundance  $n_{\text{O}} \lesssim 34 \text{ cm}^{-3}$ . As the fractional abundance of free oxygen is of the order of  $\sim 2 \times 10^{-4}$ , this implies that photodesorption cannot inhibit the formation of ices at any extinction if  $n_{\text{H}} \gtrsim 10^5 \text{ cm}^{-3}$ .

In regions where other desorption processes are significant, then the values of  $\zeta$  and  $Y_{\text{H}_2}$  will also be important. However, despite the wide variety of processes, there are not many other free parameters to which the condition for balance and  $A_{\text{th}}$  are sensitive. For example,

the freeze-out rate and all of the desorption processes listed above are all proportional to the dust surface area ( $\sigma_{\text{H}}$ ) so that its value is not of critical importance.

#### 5 THE CHEMICAL MODEL

Whilst the above arguments are useful and yield qualitative and approximate quantitative results, there are a number of inherent simplifications and approximations. For example, the abundance of oxygen atoms in equation (11) is implicitly dependent on the physical conditions, including the extinction. To unravel this degeneracy, a detailed chemical model has been applied to determine  $A_{\text{th}}$  in a self-consistent fashion.

The values of  $A_{\text{th}}$  and the slope of the water ice abundance versus  $A_V$  ( $\alpha_{\text{H}_2\text{O}}$ ) are near-universal in a specific cloud complex, indicating that the material along the lines of sight probed by the observations has reached both gas-phase and gas-grain chemical equilibrium. As such, time-dependent effects are not important in the determination of these parameters. We have therefore investigated the sensitivities of  $A_{\text{th}}$  and  $\alpha_{\text{H}_2\text{O}}$  to the physical parameters, in a model of a dynamically static cloud, evolved to chemical equilibrium (at  $t \sim 1 - 2 \times 10^6$  yr), although we have also considered the case of younger chemistries in test calculations.

The model is based on the comprehensive STARCHEM code that has been developed to study the chemistry in dynamically evolving star-forming regions, which has been successfully applied to the analysis of the chemistry of small molecular species in the pre-stellar core L1544 (Rawlings, Keto & Caselli, in preparation).

STARCHEM is a multipoint, flexible model that can be adapted to a wide range of physical and chemical descriptions. The dynamical context can either be defined analytically, or by using an interpolated grid of physical parameters in arbitrary (1D or 2D) geometry. In the current application, we simply assume a static, plane-parallel, case. Abundances are then determined for each depth point and the integrated, line of sight, column densities of H<sub>2</sub>O determined, for comparison with observations. In STARCHEM, the chemistry is dynamically switchable and includes a full description of the gas-phase, gas-grain, and surface chemistry. For the purpose of this study, we follow the depth and time-dependent evolution of the abundance of some 98 gas-phase and solid-state species, involving the elements H, He, C, N, O, S, and a representative low ionization potential metal; Na/Mg in a network of 1239 reactions (1129 gas-phase, and 110 gas-grain reactions) that gives a good description of the chemistry of small species such as H<sub>2</sub>O, CO, etc., i.e. excluding large COMs. The chemistry is taken from the UDFA data set (McElroy et al. 2013). Isothermal conditions are assumed. Although the densities are typically somewhat less than that required for the gas and dust temperatures to be well coupled, we have used a single temperature for both, noting that, for H<sub>2</sub>O and in the range of parameters that we are exploring, the results are insensitive to the value of  $T_{\text{dust}}$ . Although STARCHEM includes an integrated model of photon-dominated regions (PDRs), the values of  $A_{\text{th}}$  are  $> 2 - 3$  and so we can assume that the conditions are as appropriate to matter deep inside a PDR. We therefore assume that the photoionization rate of C and the photodissociation rates for H<sub>2</sub> and CO are negligible.

The chemistry is believed to be well evolved, as argued above, so we do not follow the time dependence of the (poorly constrained) surface chemistry. Rather, we simply assume that most of the accreting O, O<sup>+</sup>, O<sub>2</sub>, and OH are converted to H<sub>2</sub>O (subject to some desorption due to the enthalpies of formation – as described below). It is assumed that the sticking efficiency of all species is 1.0. In addition, we make some allowance for the partial ( $\sim 10$  per cent) conversion

of surface OH, in reaction with surface CO to form CO<sub>2</sub> to match the empirically determined CO<sub>2</sub>:H<sub>2</sub>O ratios in interstellar ices. So, for example, accreting oxygen atoms are converted to OH radicals, a fraction of which are returned to the gas-phase. A fraction of the remainder can react with surface CO to form surface CO<sub>2</sub>, the rest is converted to H<sub>2</sub>O and, again, a fraction of this is returned to the gas-phase, leaving the remainder as H<sub>2</sub>O ice.

In our model, we follow the procedures described in the STARCHEM model (Rawlings, Keto & Caselli, in preparation) and pay careful attention to (a) the composition of individual ice layers, and (b) the geometrical growth of grains due to ice deposition. For (a) we note that an important consequence of the ice layering/surface layer desorption scenario is that the ices act as a ‘stack’ that records and retains the prior chemical evolution of a cloud; a fact that has been used, for example, to explain the abundance anomalies in cometary ices (Rawlings, Wilson & Williams 2019). Most desorption processes only occur in the upper layer(s) of the ices, so we model the layering of the ices and follow the chemical composition of each individual layer. We then consider the two extreme examples of (i) individual layers retaining their chemical integrity (although subject to solid-state reactions taking place) – this is our standard assumption, and (ii) fully mixed ices, as would be more appropriate for non-idealized ice layering and/or disruption by heating by, for example, cosmic rays. There is no allowance for surface porosity and, other than the limited representation of the surface chemistry as described above, the ices themselves are treated as being chemically inert; that is to say we do not include the effects of chemical diffusion or mobility between layers or solid-state reactions within the ices. For (b) we make the assumption that grain growth and the increase in surface area occurs by spherically symmetric and layered accretion.

The chemical initial conditions are important and we assume that the gas starts from an essentially atomic state, but with significant conversion of H to H<sub>2</sub> (~50 per cent) and C to CO (which we treat as a free parameter). In our standard model, we assume that ~90 per cent of the carbon has been converted to CO, yielding an initial fractional abundance of CO of  $2.7 \times 10^{-4}$ .

A full description and accurate quantification of the various desorption mechanisms as described above is included in the model. In the case of H<sub>2</sub>O photodesorption, we follow Hollenbach et al. (2009) and assume that – to model the observed OH:H<sub>2</sub>O ratio in translucent clouds – the total dissociative desorption to OH + H and O + H<sub>2</sub> is twice as likely as non-dissociative photodesorption, and the total yield for the process is split accordingly.

The effect of desorption due to the enthalpy of formation of surface species is included for H<sub>2</sub> formation as an effective desorption rate with a generic (i.e. non-selective) yield for all species (as given in Table 1) and for OH and H<sub>2</sub>O formation, as a modification of the effective sticking efficiency (otherwise taken to be unity) for the O+H and OH+H surface reactions. The values used were taken from Minissale et al. (2016) and allow for the differences between reactions occurring on bare grains ( $f < 1$ ) and icy mantles ( $f > 1$ ). We do not make any other allowance for variations in  $S_{\text{eff}}$  with surface composition in our standard model. The H<sub>2</sub>O binding energy was taken to be 4800 K (Dulieu et al. 2013).

Other parameters are as specified in Table 1. Note that the adopted values of the gas and dust temperatures have a marginal effect on the gas-phase chemistry and a weak effect (through a  $T_{\text{gas}}^{1/2}$  dependence) on the freeze-out rates. The freeze-out rate of hydrogen atoms is used to evaluate the H<sub>2</sub> formation rate self-consistently. We adopt a representative gas density of  $n = 1.7 \times 10^3 \text{ cm}^{-3}$  in our standard

model. This has been chosen to give the best fit and is somewhat arbitrary: a lower value of  $n$  would result in a larger value of  $A_{\text{th}}$  (e.g. see Fig. 2), but the range of density is probably quite limited (see the discussion in section 6).

The elemental abundances have been taken from table 5 (proto-solar abundances) from Asplund et al. (2009), although the oxygen abundance has been depleted from  $5.4 \times 10^{-4}$  to a value of  $5.0 \times 10^{-4}$  (as is consistent with our understanding of the oxygen budget, e.g. Whittet (2010)). This is also chosen so as to obtain the best fit to the modelled  $A_{\text{th}}-N(\text{H}_2\text{O})$  correlation, as shown in Fig. 1, and discussed below.

## 6 RESULTS AND ANALYSIS

In the discussion that follows, we note that the essential constraints on the modelling are that the results must be consistent with (a) the observed values of  $A_{\text{th}}$ , (b) the shape and slope of the  $A_{\text{th}}-N(\text{H}_2\text{O})$  correlation ( $\alpha_{\text{H}_2\text{O}}$ ), and (c) the value of the ‘X-factor’ ( $\text{CO}/\text{H}_{\text{total}}$ ).

We make the usual assumption that the total column density for hydrogen nucleons is related to  $A_{\text{V}}$  by  $N(\text{H}/\text{cm}^{-2}) = 1.9 \times 10^{21} A_{\text{V}}$  (e.g. Whittet 2010). If we consider the observed correlation between  $A_{\text{V}}$  and  $N_{\text{H}_2\text{O}}$  given in equation (1), then the implied line of sight averaged fractional abundance of solid-state H<sub>2</sub>O is given by

$$X(\text{H}_2\text{O})_{\text{s}} \sim 1.08 \times 10^{-4} \left( 1 - \frac{2.7}{A_{\text{V}}} \right), \quad A_{\text{V}} > 2.7 \quad (12)$$

indicating that, once the threshold for ice formation has been achieved, efficient freeze-out follows (the ‘snowball’ effect). Thus,  $\alpha_{\text{H}_2\text{O}}$  is a measure of the fractional abundance of H<sub>2</sub>O in the solid state;  $X(\text{H}_2\text{O})_{\text{s}}$ . This, in turn, depends on the amount of free oxygen in the (undepleted) gas-phase, most of which is subsequently converted to H<sub>2</sub>O ice. Unfortunately, this quantity is hard to estimate since (i) it will depend, in part, on the efficiency of conversion of C to CO, which is a relatively slow process, and (ii) there is a significant component of the interstellar oxygen budget that is unaccounted for. This component possibly accounts for in excess of 50 per cent of the total that is not included in the silicate/oxide dusts and may reside in some form of oxygen-bearing carbonaceous matter (Whittet, 2010).

Even allowing for this, at least 25 per cent of the remaining oxygen is taken up in the form of CO, if we assume that significant C-to-CO conversion has occurred. In dark clouds in the Milky Way it is usually reasonable to assume that this is a correct assumption, yielding a mean CO-to-H<sub>2</sub> conversion factor of  $X_{\text{CO}} \sim 2 \times 10^{20} \text{ cm}^{-2} (\text{K kms}^{-1})$ . However, there is some variation from sight line to sight line. In clouds with relatively low extinctions (i.e.  $A_{\text{V}} \sim 0.37\text{--}2.5 \text{ mag}$ , so that they are at or near the threshold for CO detection, below which the emission region is classified as dark molecular gas)  $X_{\text{CO}}$  can be 6–7 times larger, suggesting that C-to-CO conversion is incomplete (Luo et al. 2020) in these sources. This may explain some of the scatter in the data points, particularly in the vicinity of  $A_{\text{V}} = A_{\text{th}}$ .

### 6.1 $N(\text{H}_2\text{O})$ versus $A_{\text{V}}$

Results from the model are presented in two forms; as shown in Figs 1 and 2. In Fig. 1, we show the calculated late-time (equilibrium) values of the H<sub>2</sub>O ice column density as a function of  $A_{\text{V}}$  (calculated in 50 independent model calculations; spanning the range of extinctions  $1 < A_{\text{V}} < 5.9$ ) for variations in the free parameters, at a fixed density of  $1700 \text{ cm}^{-3}$ .

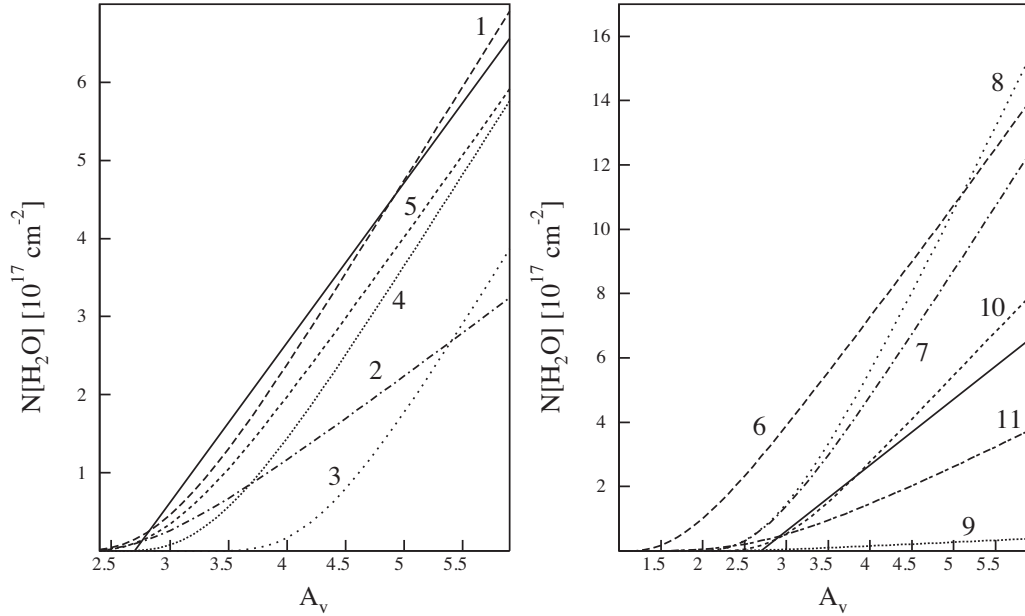


**Figure 1.** The modelled late-time column densities of water ice as a function of extinction,  $A_V$ . The labels refer to the model number, whose details are given in Table 2. The solid line in both plots is the empirical correlation (from data presented in Whittet et al. 2013).

Although there are a large number of parameters in the model, only a relatively small subset of these have significant effects on  $A_{\text{th}}$  and/or the slope of the  $A_V$ – $N(\text{H}_2\text{O})$  correlation for a given value of the density. These are  $X(\text{O})_{\text{total}}$  or  $X(\text{CO})_0$ ,  $G$ ,  $Y_{\text{pd}}$ ,  $Y_{\text{H}_2}$  (and the chemical desorption yields for OH and  $\text{H}_2\text{O}$  formation),  $\sigma_{\text{H}}$ , and  $\zeta$ . We consider the effects of variations in these parameters in models 1–11, whose details are specified in Table 2.

As can be seen from Fig. 1, the standard model (no. 1) gives a good fit to  $A_{\text{th}}$ ,  $\alpha_{\text{H}_2\text{O}}$ , and the shape of the  $N(\text{H}_2\text{O})$ – $A_V$  correlation although, as explained above, the initial value of the oxygen atom abundance was chosen to obtain the best fit to  $\alpha_{\text{H}_2\text{O}}$ .

If we do not take into account the geometrical effects of ice mantle growth as would be appropriate for larger grain sizes, a very poor fit to  $\alpha_{\text{H}_2\text{O}}$  is obtained (model 2) and cannot be rectified by changes in the other free parameters. Increasing the radiation field strength (model 3) or using slightly higher photodesorption yields (model 4; for which  $Y_{\text{pd}} = 2 \times 10^{-3}$  and  $Y_{\text{pd-cr}} = 3 \times 10^{-3}$  for the direct and cosmic-ray-induced processes respectively, as used in Kalvāns 2015) both strongly affect  $A_{\text{th}}$ , although the effects on  $\alpha_{\text{H}_2\text{O}}$  are quite small. Introducing  $\text{H}_2$  formation-driven desorption with even a very small yield (model 5) also has a clearly discernable effect on  $A_{\text{th}}$ . Increasing the density (model 6) results in a significant reduction in  $A_{\text{th}}$ , although the effect on  $\alpha_{\text{H}_2\text{O}}$  is relatively small. Conversely, the non-inclusion of  $\text{H}_2\text{O}$  formation-driven desorption (model 7) or variations in the initial oxygen atom abundance (as controlled by the initial abundance of CO; model 8) both have strong effects on  $\alpha_{\text{H}_2\text{O}}$ , although less so on  $A_{\text{th}}$ . Reducing the chemical age to  $10^5$  yr dramatically inhibits ice formation at all extinctions (model 9). As expected, the results are not strongly sensitive to the value of  $\sigma_{\text{H}}$  (model 10), but reducing the efficiency of the (solid state) conversion of O-to- $\text{H}_2\text{O}$  results in significant reductions of both  $A_{\text{th}}$  and  $\alpha_{\text{H}_2\text{O}}$  (model 11).

In additional calculations (not shown in Fig. 1), we found that increasing the cosmic ray ionization rate by a factor of 5–10× had very little effect on the results. Also, if we arbitrarily reduce the sticking efficiency for oxygen (and other species) from 1.0 to 0.5, then  $A_{\text{th}}$  is raised by  $\sim 0.5$  and  $\alpha_{\text{H}_2\text{O}}$  is significantly reduced.

## 6.2 The dependence of $A_{\text{th}}$ on the free parameters

For Fig. 2, we have performed a large grid of calculations in  $(A_V, n_{\text{tot}})$ -space, covering the range  $1 < A_V < 10.5$  and  $2 < \log_{10} n < 4.5$ , again evolved until  $t = 1 - 2 \times 10^6$  yr. Calculations have been made for different values of the free parameters to which  $A_{\text{th}}$  is most sensitive. The curves in the figures show the locus of points on the  $(A_V, n_{\text{tot}})$  plane corresponding to the conditions yielding  $f_{\text{H}_2\text{O}} = 1$ , which, as argued above, approximately corresponds to  $A_V = A_{\text{th}}$ . This figure therefore shows the dependence of the modelled values of  $A_{\text{th}}$  on the local density ( $n$ ), and how that dependence is sensitive to variations in other key free parameters. The parameters/ranges that we have investigated and presented in the figure are (a) radiation field strength:  $G = 0.5 - 20$ , (b) photodesorption yields:  $Y_{\text{pd}} = 10^{-4} - 10^{-2}$ , (c) cosmic ray ionization rate:  $\zeta = 10^{-18} \text{s}^{-1} - 10^{-16} \text{s}^{-1}$ , and (d)  $\text{H}_2$ -formation driven desorption yield:  $Y_{\text{H}_2} = 0 - 10^{-3}$ .

First, in all of the plots we note the sensitivity of  $A_{\text{th}}$  to the density ( $n$ ); an increase in density of a factor of  $\sim 10$  results in a reduction of  $A_{\text{th}}$  by  $\sim 1.5$  magnitudes. Secondly, in most cases, no stable solution can be found for  $A_{\text{th}} \gtrsim 6 - 6.5$ . As expected, the correlations are seen to be sensitive to the values of  $G$  and  $Y_{\text{pd}}$ , although to obtain a value of  $A_{\text{th}}$ , as is appropriate for Serpens a very low density  $\lesssim 150 \text{ cm}^{-3}$  is required. The dependencies on  $\zeta$  and  $Y_{\text{H}_2}$  are very much weaker. Large values of  $Y_{\text{H}_2}$  ( $\gtrsim 5 \times 10^{-4}$ ) result in significant modifications of the required minimum density for ices to form.

## 6.3 The dependence on density

The sensitivity of  $A_{\text{th}}$  to the density is hard to reconcile with the fact that  $A_{\text{th}}$  is very similar along different lines of sight unless the range of volume density is limited, and/or the volume density is closely correlated to the column density, which implies a self-similar evolution of the various cores that are probed along different lines of sight.

We have already noted (in section 4) that the balance between photodesorption and freeze-out requires that the density  $< 10^5 \text{ cm}^{-3}$ . In addition, the uniformity of  $\alpha_{\text{H}_2\text{O}}$  implies that the freeze-out and

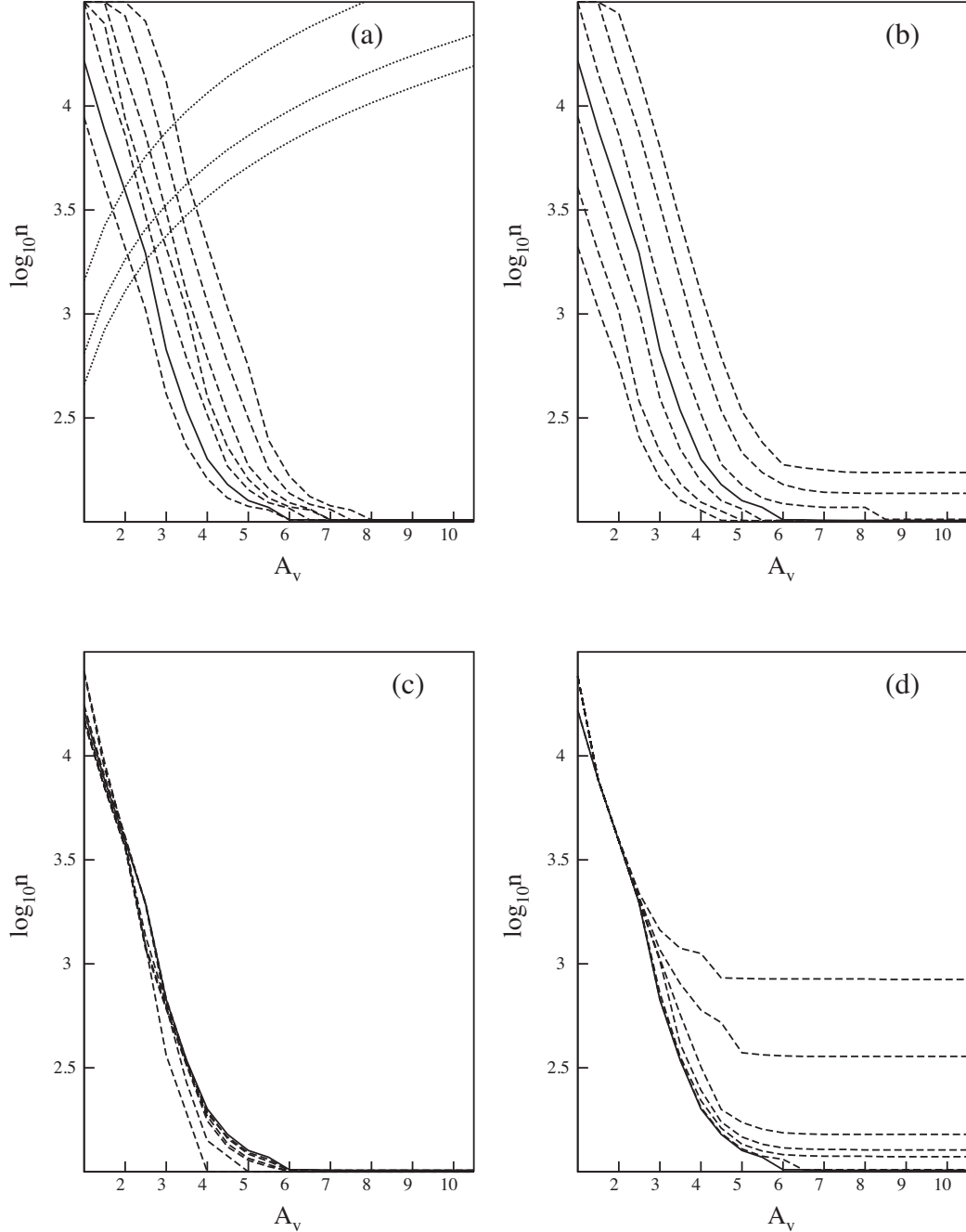


**Figure 2.** The locus of points  $(A_V, n_{\text{tot}})$  for which  $A_V = A_{\text{th}}$ . The additional parameter that is varied in each plot, and the values for the curves (from bottom left to top right) are (a)  $G = 0.5, 1, 2, 3, 5, 10,$  and  $20$ , (b)  $Y_{\text{pd}}$  (in units of  $10^{-4}$ ) =  $1, 2, 5, 10, 20, 50,$  and  $100$ , (c)  $\zeta =$  (in units of  $10^{-17} \text{s}^{-1}$ ) =  $0.1, 0.2, 0.5, 1.3, 2, 5,$  and  $10$ , (d)  $Y_{\text{H}_2}$  (in units of  $10^{-4}$ ) =  $0, 0.1, 0.5, 1, 2, 5,$  and  $10$ . The values corresponding to our standard model (1) are represented by the solid line in each plot. The dotted lines in (a) show the correlation between density ( $n$ ) and extinction ( $A_V$ ) in the case of homologous collapse of uniform cores (from top to bottom) of masses  $2, 10,$  and  $20 M_{\odot}$ .

desorption processes are in quasi-equilibrium. The time-scale for freeze-out (given by equation 3) then implies that, for a reasonable upper limit of the cloud age of  $\sim 10$  Myr, the density is  $\gtrsim 3 \times 10^2 \text{ cm}^{-3}$  in the regions probed by the observations.

This range of densities could be restricted further if we consider cloud structure and evolutionary state. It is possible that the local density ( $n_{\text{H}}$ ) and  $A_V$  (and hence the column density  $N_{\text{H}}$ ) could be correlated if we assume that the lines of sight pass through clumps/cores in varying states of evolution. We can estimate this by assuming that each core is spherical, has a uniform density and contracts homologously (the approximate situation in the very

earliest stages of collapse), in which case the column density and volume density of a core of mass  $M$  are simply related by

$$N = \left( \frac{6M}{\pi \mu m_{\text{H}}} \right)^{1/3} n^{2/3}. \quad (13)$$

Assuming that the correlation between  $N_{\text{H}}$  and  $A_V$  holds, this implies that

$$A_V \sim 0.62 \left( \frac{M}{M_{\odot}} \right)^{1/3} \left( \frac{n}{1000 \text{ cm}^{-3}} \right)^{2/3}. \quad (14)$$

**Table 2.** Parameter variations used in models 1–11.

Model number	Parameter	Value
1	Standard	–
2	$\Delta a$	0 (no grain growth)
3	$G$	10.0
4	$Y_{\text{pd}}/Y_{\text{pd-cr}}$	$2.0 \times 10^{-3}/3.0 \times 10^{-3}$
5	$Y_{\text{H}_2}$	$2.0 \times 10^{-4}$
6	$n$	$1 \times 10^4 \text{cm}^{-3}$
7	–	no H <sub>2</sub> O formation desorption
8	$X(\text{CO})_0$	$1.0 \times 10^{-6}$
9	Age	$10^5$ years
10	$\sigma_{\text{H}}$	$5 \times 10^{-21} \text{cm}^2$
11	O→H <sub>2</sub> O efficiency	0.5

We have plotted the correlation given by equation (14) in Fig. 2 for the cases of  $M = 2, 10, \text{ and } 20 M_{\odot}$ . What this shows is that, for our standard model – with this additional constraint for this range of core masses – the upper limit of the density is significantly reduced to  $\sim 4 \times 10^3 \text{cm}^{-3}$  and the value of  $A_{\text{th}}$  lies in the relatively narrow range of  $\sim 2\text{--}2.7$  (and is perhaps indicative of a slightly higher value of  $G \sim 2$ ).

If the cores are more evolved than this simple uniform density representation, then their internal structures will be closer to that of Bonnor–Ebert spheres, but a similar dependence would result, with a somewhat different scaling factor. In any case, these results indicate that, although there are a large number of free parameters in the model, they are all fairly well constrained to lie within relatively narrow ranges.

As a caveat, we note that the situation could be further complicated if we recognize that  $A_{\text{V}} > A_{\text{th}}$  in the innermost parts of cores, in which case line of sight filling factors must be taken into account.

## 6.4 Summary of results

In broad terms, the resulting dependencies on the free parameters in the model are found to be as follows:

(i) The value of  $A_{\text{th}}$  is, as expected, strongly sensitive to (a) the radiation field strength ( $G$ ), (b) the yields for the photodesorption processes, and (c) the local density.

(ii)  $A_{\text{th}}$  has a weaker dependence on the abundance of free oxygen, and the assumed H<sub>2</sub>O formation-driven desorption and surface hydrogenation efficiencies.

(iii) Other than variations in the intrinsic microphysics (e.g. the dust grain surface area per hydrogen nucleon, and whether or not ice mantle growth is taken into account, the efficiencies of H<sub>2</sub>O formation-driven desorption and surface hydrogenation reactions), the slope of the  $N(\text{H}_2\text{O})\text{--}A_{\text{V}}$  correlation ( $\alpha_{\text{H}_2\text{O}}$ ) is only sensitive to the initial abundance of free oxygen atoms and the assumption of chemical equilibrium (i.e. the chemical age).

(iv) The assumption of no grain growth due to ice mantle accretion (which is close to being accurate in the case of an assumed larger initial mean grain radius) results in a large reduction of  $\alpha_{\text{H}_2\text{O}}$ .

## 7 ALTERNATIVE MECHANISMS

In this section, we investigate two other possible mechanisms that may explain the  $A_{\text{th}}$  phenomenon, which are not directly related to the  $A_{\text{V}}$ -dependence of photodesorption. Both of these rely on variations in the binding energy of H<sub>2</sub>O to dust grains.

The empirical basis for the determination of desorption rates are generally based on laboratory experiments involving pure or mixed multilayer ices that cover idealized carbon (graphitic, metallic) substrates. However, if we consider both (a) the low surface coverage (sub-monolayer), or (b) different forms of the substrate, then significant variations in the net sticking efficiency for oxygen atoms may result.

### 7.1 Threshold coverage for hydrogen bonding

First, we speculate that the onset of ice deposition at a particular visual extinction is determined by the requirement that the flux of impinging atoms must exceed some critical value so as to maintain a significant surface coverage of ice. The assumption is that lone H<sub>2</sub>O molecules are relatively weakly bound to the surface and can readily be desorbed by various mechanisms, whereas bulk water ice is bound by relatively much stronger hydrogen bonding, in addition. Thus, for ice to be formed, the O atom flux at the surface of grains must be large enough to overcome any desorbing mechanisms, by establishing a surface density of H<sub>2</sub>O molecules above some critical value.

We can simulate this process, in effect, by enhancing the desorption rates if the abundance of H<sub>2</sub>O in the sub-monolayer regime is less than some critical value,  $f_{\text{H}_2\text{O,crit}}$ . To test this, we have performed calculations where we (arbitrarily) enhance all of the desorption rates by factors of (i)  $10\times$  and (ii)  $100\times$  in the sub-monolayer regime, and take the extreme example of  $f_{\text{H}_2\text{O,crit}} = 1$ . In practice, this has to be applied to all species, and not just H<sub>2</sub>O, otherwise ices of CH<sub>4</sub>, NH<sub>3</sub>, and CO etc. rapidly establish a monolayer and the effect is fairly minimal, even if the desorption enhancement is applied to the top three monolayers. Applying the enhancement to all species results in a significant increase in the values of  $A_{\text{th}}$  (e.g. to 4.4 and 5.6 for models 1 and 3, respectively, for case i). For case (ii) ices never form at any value of  $A_{\text{V}}$  for models 1–5. However, in all models the situation rapidly switches once  $f_{\text{H}_2\text{O,crit}}$  has been obtained and the usual  $N(\text{H}_2\text{O})\text{--}A_{\text{V}}$  correlation ensues. This yields a discontinuous curve that is at odds with the observations. We therefore conclude that this process is probably not important.

### 7.2 The dependence of H<sub>2</sub>O bonding with grain surface on $A_{\text{V}}$

The nature of the surface of dust grains changes with depth into a cloud, and here we speculate that this may affect the binding energy of H<sub>2</sub>O to the surface. Interstellar dust is conventionally assumed to be composed predominantly of silicates or carbons. Experimental and theoretical studies of H<sub>2</sub>O binding energies are mostly limited to carbons, in particular to graphitic (sp<sup>2</sup>) carbon. This may not be too great a restriction, as in some models of interstellar dust, much of the carbon is assumed to be in the form of a layer on silicate substrates rather than free-flying carbon grains (e.g. Jones, Duley & Williams 1990). If so, then the H<sub>2</sub>O-silicate interaction is of lesser importance.

However, hydrogenated amorphous carbon may adopt several kinds of chemical bonding, including sp<sup>2</sup> (graphitic) and sp<sup>3</sup> (polymeric); the bonding affects the physical and chemical properties of the solid. Conversions between these and other types of carbon may be induced by UV irradiation (photodarkening; sp<sup>3</sup> → sp<sup>2</sup>) and by hot H atom (and C/C<sup>+</sup> atom) insertion (sp<sup>2</sup> → sp<sup>3</sup>). Thus, interstellar carbons may be expected to change their nature according to their environment (Jones et al. 1990). Detailed studies (e.g. Cecchi-Pestellini et al. 2010) show that for typical interstellar cloud conditions the bulk of the carbon on a silicate grain is sp<sup>2</sup>; however, much of the carbon surface layer is sp<sup>3</sup>. For molecular clouds, after

a reasonable evolution time ( $\sim 10^5$  yr) a phase transition between  $sp^2$  and  $sp^3$  occurs in the surface layer at depths into a cloud of about 3 mag.  $H_2O$  is likely to have a lower binding energy with  $sp^2$  carbon than it does with hydrogenated  $sp^3$  carbon, via hydrogen bonding. It is therefore possible that this phase transition may affect the deposition of  $H_2O$  on interstellar dust, and it is interesting to note that the transition occurs at depths similar to values of  $A_{th}$  in nearby interstellar clouds.

Unfortunately, whilst the binding energy of  $H_2O$  on graphite and other  $sp^2$  surfaces has been well determined and forms the basis of empirical studies of laboratory simulations of interstellar gas-grain interactions, the binding energy on polymeric carbon ( $sp^3$ ) is currently unknown and so we are not able to quantify the effect. However, we note that, unlike the other mechanisms discussed in this paper, this provides a possible explanation for the  $A_{th}$  phenomenon that is unrelated to the  $A_V$ -dependence of photodesorption.

## 8 CONCLUSIONS

First, we should note that there are several simplifications and assumptions that we have made in this paper:

(i) Although we have considered grain growth by ice mantle accretion and its regulation of the freeze-out and desorption processes, we have not included the effect that such grain growth will have on the UV extinction and how that would modify the dependence of photoprocesses (including photodesorption) on  $A_V$ . Thus, for example, in our standard model once  $A_V \sim 4$ ,  $\sim 18$  ice layers will have been accreted, implying an ice mantle thickness of  $\sim 70$  Å. This effectively eliminates the population of particles with sizes  $50$  Å  $< a < 120$  Å from the distribution and would, inevitably, result in a significant reduction of the extinction in the UV.

(ii) We have not included the effects of changes in the grain albedo as ices build-up. There is indeed evidence for a change in the optical properties of the dust as the density increases (Whittet et al. 2013) and such changes could result in significant variations in the cosmic ray induced photon flux and photodesorption rates.

(iii) We have treated clouds as plane-parallel and have not included any representation of the internal density structure. We could, for example, speculate an alternative theory for the origin of the  $N(H_2O)$ - $A_V$  correlation that is based on the observational evidence that clouds contain transient microstructure (Girart et al. 2002; Hartquist, Falle & Williams 2003; Garrod, Williams & Rawlings 2006). The densities in the microstructure appear to be high enough for freeze-out to be rapid. In this picture, a dark cloud may be considered as a collection of dense clumps embedded in a lower density background gas, some of which may be gravitationally bound and subsequently collapse to form stars. The ice would be entirely contained within these clumps, which may be intersected by a line of sight passing through the cloud. Thus,  $N(H_2O)$  would be determined by the clump filling factor in the observational beam and/or the number of clumps that intersect the line of sight, and  $\alpha_{H_2O}$  would be determined by the density and distribution of clumps.

However, despite these assumptions and limitations, we can draw some important conclusions from this study. Our main findings are as follows:

(i) The fact that  $A_{th} \sim 3.2$  in several quiescent regions (Taurus, Elias 16, IC 5146) is remarkable and points to a common cause that is neither time dependent, nor sensitive to local variations of physical conditions.

(ii) We have shown that the astronomical data for  $A_{th}$  and  $\alpha_{H_2O}$  are not only powerful probes of the physical conditions within dark interstellar clouds but also constrain the poorly known microphysics of ice deposition in those regions.

(iii) The existence of  $A_{th}$  can be explained as being due to the balance between freeze-out and photodesorption for these sources. No other desorption mechanism (even the more speculative ones) is capable of explaining the phenomenon.

(iv) We have investigated two other mechanisms as possible causes of the  $A_{th}$  phenomenon, in which the effective binding energy of  $H_2O$  molecules is determined by (i) the requirement of a critical surface density of  $H_2O$ , or (ii) the nature of the surface layers of carbon ( $sp^2$  or  $sp^3$ ). We find that the first of these can result in significant variations in  $A_{th}$ , but is still subject to the same constraints as simple photodesorption, and predicts an incorrect shape to the  $A_V$ - $N(H_2O)$  correlation. The second is viable, and is largely independent of the photodesorption constraints, but is – as yet – unquantifiable.

(v) In addition to  $A_{th}$ , the near-linear shape and slope ( $\alpha_{H_2O}$ ) of the correlation between the extinction and the inferred  $H_2O$  ice column density is also very similar along different lines of sight. This implies that the observations probe clouds in remarkably similar dynamical and chemical evolutionary states. Our model yields a very good match to the value of  $A_{th}$ ,  $\alpha_{H_2O}$  and the shape of the  $A_V$ - $N(H_2O)$  correlation. However, the values of  $A_{th}$  and  $\alpha_{H_2O}$  are affected by the values of the key free parameters that we have investigated in our models (most notably the density, the radiation field strength, the oxygen abundance, and the characteristics of the dust grain physics and surface chemistry), implying that none of them can vary significantly along different lines of sight in the Taurus complex.

(vi) The near linear shape of the  $A_V$ - $N(H_2O)$  correlation is consistent with the fact that the bulk of the ice grows on (initially) very small dust grains ( $a < 0.01$   $\mu m$ ).

(vii) Once ice starts to be deposited, then it rapidly builds up to saturation levels, containing almost all of the available oxygen that is not bound in CO or organic or refractory components. The shape and slope of the  $A_V$ - $N(H_2O)$  correlation indicates that the clouds are well evolved (with ages  $>> 10^5$  yr) and with a uniform net free oxygen abundance (prior to freeze-out) of  $\sim 2.3 \times 10^{-4}$  (indicating efficient conversion of C to CO).

(viii) The only ways in which significantly larger values of  $A_{th}$  can be obtained are (i) by increasing the ambient radiation field strength ( $G$ ), (ii) increasing the photodesorption yields ( $Y_{pd}$ ), and/or (iii) reducing the density ( $n$ ). The value of  $A_{th}$  is only sensitive to these parameters. The differences between  $A_{th}$  in Taurus and Serpens can probably best be explained by differences in  $G$ . Although less likely as the cause, the differences could possibly originate from extreme variations in the dust composition and hence the desorption yields.

(ix) By contrast, the very high value of  $A_{th} \sim 10$ – $15$  that is determined for  $\rho$ -Oph cannot be explained so simply; photodesorption by secondary (cosmic ray induced) photons would be the more significant mechanism at extinctions significantly less than these values. The fact that there is a correlation between  $A_V$  and  $N_H$  indicates that some other process is important.  $\rho$ -Oph is more dynamically active than Taurus or Serpens, so that internal heating sources may be important.

Alternatively, it is possible that UV photons could penetrate deep inside a cloud if the extinction is anomalous in the far-UV rise. In dense gas, the effects of both ice mantle accretion and dust coagulation become effective and the relative absence of small dust grains could greatly enhance the UV field strength at much higher  $A_V$  values than normal.

(x)  $A_{\text{th}}$  has a fairly strong dependence on the gas density that implies that the range of densities probed by observations is restricted and/or there is a correlation between volume and column densities. The requirements of chemical equilibrium and the balance between photodesorption and freeze-out set some constraints on the density range, but this is significantly restricted if the assumption is made that the cores are in different stages of evolution along a similar evolutionary track. The universality of  $A_{\text{th}}$  and  $\alpha_{\text{H}_2\text{O}}$  is therefore remarkable as it implies that, averaged over the various lines of sight, there must be near-universal laws of morphological/density structure and evolution within the cloud complexes.

## DATA AVAILABILITY

The data underlying this study are openly available from the published papers that are cited in the article. No new data were generated in support of this research.

## REFERENCES

- Andersson S., van Dishoeck E. F., 2008, *A&A*, 491, 907  
 Asplund M., Grevesse N., Sauval A. J., Scott P., 2009, *ARA&A*, 47, 481  
 Bergin E., Melnick G. J., Gerakines P. A., Neufeld D. A., Whittet D. C. B., 2005, *ApJ*, 627, L33  
 Cecchi-Pestellini C., Cacciola A., Iati M. A., Saija R., Borghese F., Denti P., Giusto A., Williams D. A., 2010, *MNRAS*, 408, 535  
 Chiar J. E., Adamson A. J., Kerr T. H., Whittet D. C. B., 1994, *ApJ*, 426, 240  
 Chiar J. E. et al., 2007, *ApJ*, 666, L73  
 Chiar J. E. et al., 2011, *ApJ*, 731, 9  
 Cuppen H. M., Herbst E., 2007, *ApJ*, 668, 294  
 Cuppen H. M., Ioppolo S., Romanzin C., Linnartz H., 2010, *Phys. Chem. Chem. Phys.*, 12, 12077  
 Du F., Parise B., Bergman P., 2012, *A&A*, 538, A91  
 Dulieu F., Congiu E., Noble J., Baouche S., Chaabouni H., Moudens A., Minissale M., Cazaux S., 2013, *Nature Sci. Rep.*, 3, 1338  
 Hodapp E., 1989, *A&A*, 201, 354  
 Garrod R. T., Williams D. A., Rawlings J. M. C., 2006, *ApJ*, 638, 827  
 Gillett F. C., Forrest W. J., 1973, *ApJ*, 179, 483  
 Girart J. M., Viti S., Williams D. A., Estalella R., Ho P. T. P., 2002, *A&A*, 388, 1004  
 Hartquist T. W., Falle S. A. E. G., Williams D. A., 2003, *ApSpSci*, 288, 369  
 Hasegawa T., Herbst E., 1993, *MNRAS*, 261, 83  
 Hollenbach D., Kaufman M. J., Bergin E. A., Melnick G. J., 2009, *ApJ*, 690, 1497  
 Ioppolo S., Cuppen H. M., Romanzin C., 2008, *ApJ*, 686, 1474  
 Jones A. P., Williams D. A., 1984, *MNRAS*, 209, 955  
 Jones A. P., Duley W. W., Williams D. A., 1990, *QJRAS*, 31, 567  
 Kalvāns J., 2015, *ApJ*, 803, 52  
 Lamberts T., Cuppen H. M., Ioppolo S., Linnartz H., 2013, *Phys. Chem. Chem. Phys.*, 15, 8287  
 Leto G., Baratta G. A., 2003, *A&A*, 397, 7  
 Luo G. et al., 2020, *ApJ*, 889, L4  
 Mathis J. S., Rumpl W., Nordsieck K. H., 1977, *ApJ*, 217, 425  
 McElroy D., Walsh C., Markwick A. J., Cordiner M. A., Smith K., Millar T. J., 2013, *A&A*, 550, A36  
 Minissale M., Dulieu F., Cazaux S., Hocuk S., 2016, *A&A*, 585, A24  
 Noble J. A., Fraser H. J., Aikawa Y., Pontoppidan K. M., Sakon I., 2013, *ApJ*, 775, 85  
 Öberg K. I., Linnartz H., Visser R., van Dishoeck E. F., 2009, *ApJ*, 693, 1209  
 Prasad S. S., Tarafdar S. P., 1983, *ApJ*, 267, 603  
 Rawlings J. M. C., Hartquist T. W., Menten K., Williams D. A., 1992, *MNRAS*, 255, 471  
 Rawlings J. M. C., Wilson T. G., Williams D. A., 2019, *MNRAS*, 486, 10  
 Roberts J. F., Rawlings J. M. C., Viti S., Williams D. A., 2007, *MNRAS*, 382, 733  
 Tanaka M., Sato S., Nagata T., Yamamoto T., 1990, *ApJ*, 352, 724  
 Taquet V., Ceccarelli C., Kahane C., 2012, *A&A*, 538, A42  
 van Dishoeck E. F., Herbst E., Neufeld D., 2013, *Chem. Rev.*, 113, 9043  
 Westley M. S., Baragiola R. A., Johnson R. E., Baratta G. A., 1995, *Nature*, 373, 405  
 Whittet D. C. B., 2003, *Dust in the Galactic Environment*. IoP Publishing, Bristol  
 Whittet D. C. B., 2010, *ApJ*, 710, 1009  
 Whittet D. C. B., Blades J. C., 1980, *MNRAS*, 190, 403  
 Whittet D. C. B., Adamson A. J., Duley W. W., Geballe T. T., McFadzean A. D., 1989, *MNRAS*, 241, 707  
 Whittet D. C. B., Gerakines P. A., Hough J. H., Shenoy S. S., 2001, *ApJ*, 547, 872  
 Whittet D. C. B., Shenoy S. S., Bergin E. A., Chiar J. E., Gerakines P. A., Gibb E. L., Melnick G. J., Neufeld D. A., 2007, *ApJ*, 655, 332  
 Whittet D. C. B., Cook A. M., Chiar J. E., Pendleton Y. J., Shenoy S. S., Gerakines P. A., 2009, *ApJ*, 695, 94  
 Whittet D. C. B., Poteet C. A., Chiar J. E., Pagani L., Bajaj V. M., Horne D., Shenoy S. S., Adamson A. J., 2013, *ApJ*, 774, 102  
 Williams D. A., Hartquist T. W., Whittet D. C. B., 1992, *MNRAS*, 258, 599  
 Yabushita A., Kanda D., Kawanaka N., Kawasaka M., Ashfold M. N. R., 2006, *J. Chem. Phys.*, 125, 3406

This paper has been typeset from a  $\text{\TeX}/\text{\LaTeX}$  file prepared by the author.